

# Preservation of Surface Conductivity and Dielectric Loss Tangent in Large-Scale, Encapsulated Epitaxial Graphene Measured by Noncontact Microwave Cavity Perturbations

Albert F. Rigosi,\* Nicholas R. Glavin, Chieh-I Liu, Yanfei Yang, Jan Obrzut, Heather M. Hill, Jiuning Hu, Hsin-Yen Lee, Angela R. Hight Walker, Curt A. Richter, Randolph E. Elmquist, and David B. Newell

**R**egarding the improvement of current quantized Hall resistance (QHR) standards, one promising avenue is the growth of homogeneous monolayer epitaxial graphene (EG). A clean and simple process is used to produce large, precise areas of EG. Properties like the surface conductivity and dielectric loss tangent remain unstable when EG is exposed to air due to doping from molecular adsorption. Experimental results are reported on the extraction of the surface conductivity and dielectric loss tangent from data taken with a noncontact resonance microwave cavity, assembled with an air-filled, standard R100 rectangular waveguide configuration. By using amorphous boron nitride (a-BN) as an encapsulation layer, stability of EG's electrical properties under ambient laboratory conditions is greatly improved. Moreover, samples are exposed to a variety of environmental and chemical conditions. Both thicknesses of a-BN encapsulation are sufficient to preserve surface conductivity and dielectric loss tangent to within 10% of its previously measured value, a result which has essential importance in the mass production of millimeter-scale graphene devices demonstrating electrical stability.

Graphene, the atomically thin layer of carbon atoms arranged in a hexagonally tiled lattice, has been shown to possess fantastic electrical properties.<sup>[1–3]</sup> One specific and interesting avenue of research involves the epitaxial growth of graphene on silicon carbide (SiC), which displays properties thought to be advantageous for the development of a quantized Hall

resistance (QHR) standard.<sup>[4–10]</sup> One of the foundational concepts to the QHR is that the  $\nu=2$  plateau in the quantum Hall effect (QHE), observed in epitaxially grown graphene (EG), becomes accessible at lower fields, higher temperatures, and higher currents than materials whose 2D electron gas systems have been previously measured for QHR standards, such as

Dr. A. F. Rigosi, C.-I. Liu, Dr. Y. Yang, Dr. J. Obrzut,  
Dr. H. M. Hill, Dr. J. Hu, Dr. H.-Y. Lee, Dr. A. R. Hight Walker,  
Dr. C. A. Richter, Dr. R. E. Elmquist, Dr. D. B. Newell  
National Institute of Standards and Technology (NIST)  
100 Bureau Drive, Gaithersburg, MD 20899, USA  
E-mail: albert.rigosi@nist.gov

Dr. N. R. Glavin  
Materials and Manufacturing Directorate  
Air Force Research Laboratory  
Wright-Patterson AFB  
OH 45433, USA

C.-I. Liu  
Graduate Institute of Applied Physics  
National Taiwan University  
Taipei 10617, Taiwan  
Dr. Y. Yang  
Joint Quantum Institute  
University of Maryland  
College Park, MD 20742, USA  
Dr. H.-Y. Lee  
Theiss Research  
La Jolla, CA 92037, USA



DOI: 10.1002/sml.201700452

The ORCID identification number(s) for the author(s) of this article can be found under <https://doi.org/10.1002/sml.201700452>.

GaAs-AlGaAs heterostructures<sup>[11]</sup> and silicon metal-oxide-semiconductor field-effect transistors.<sup>[12]</sup> Experiments performed on millimeter-sized EG are assuring indications that mass fabrication of graphene-based QHR standards are quite feasible and could be disseminated.<sup>[13–15]</sup> Although the surface conductivity and dielectric loss tangent are good noncontact properties by which to assess the quality of the EG, it is imperative to the eventual development of a reliable QHR that the stability of these properties is established.

Generally, EG quality, determined by a few different quantities including the surface conductivity and dielectric loss tangent, is unstable over time when kept in ambient air conditions.<sup>[16–19]</sup> This incentive to stabilize properties of EG motivates the efforts to encapsulate EG with an electrical insulator. Applications to general engineering of electronics, sensors, and 2D devices may be realized upon being able to preserve the reliability of QHE measurements. This reliability would be one direct consequence of preserving the measurable quantities on which the mechanisms of the QHE depend. Some recent studies explore the effects of poly methyl methacrylate-based polymer encapsulation on EG<sup>[20]</sup> as well as general influences of dielectrics deposited by atomic layer deposition.<sup>[21–24]</sup>

Although recent aforementioned efforts encapsulate EG successfully, few experiments have been conducted showing that large-area (e.g., millimeter scale) depositions of boron nitride can be successfully implemented as a preserving agent. Encapsulation has been widely practiced with mechanically exfoliated hexagonal boron nitride (*h*-BN), but the lateral size constraint of a few hundred micrometers per piece of *h*-BN renders any attempts to encapsulate millimeter-sized areas with this technique as impractical. Recent studies' utilization of pulsed laser deposition allows for different structural forms of boron nitride to form a thin film on a substrate of interest.<sup>[25–27]</sup> Amorphous boron nitride (*a*-BN) is used in this work as a means to encapsulate large areas of EG and is performed at temperatures around 200 °C.

Recent efforts to mass-characterize large-scale EG include those that utilize a microwave cavity to record electromagnetic perturbations caused by inserting a sample into a rectangular waveguide. Subsequently, those data are processed to yield the surface conductivity of the inserted sample.<sup>[28–30]</sup>

EG samples were grown on 7.6 mm by 15.1 mm rectangular SiC chips diced from 4H-SiC(0001) semi-insulating wafers (CREE<sup>[31]</sup>). More details are provided in Table S1 of the Supporting Information. A graphite-lined resistive-element furnace (Materials Research Furnaces Inc.<sup>[31]</sup>) is used for epitaxial growth, where heating and cooling rates are typically 1.5 °C s<sup>-1</sup>. The chamber is flushed with Ar gas, and filled with 80 kPa Ar from a 99.999% liquid Ar source before annealing at 1900 °C. Upon completion of EG growth on the SiC chips, a clean fabrication process, using gold as a protecting layer, allows for etching a well-defined, rectangular area of graphene. For reasons to be specified later in this work, this well-defined shape is necessary to help simplify the process of analyzing data from the microwave cavity.

After initial processing, the samples are examined under a microscope and their images are recorded. Raman spectra are also obtained to verify the quality of the graphene. The

results of this characterization are included in the Supporting Information. An initial set of microwave cavity measurements are taken, whose details are described later on. *a*-BN encapsulation then takes place in a home-built vacuum chamber that is pumped down to at least 10<sup>-6</sup> Pa. More details regarding the growth and properties of *a*-BN thin films are currently available in previous manuscripts.<sup>[23,25]</sup> The deposition begins with the ablation of a high purity amorphous BN target with a KrF laser in 6.66 Pa of ultra-high pressure nitrogen gas. Due to the ablated plasma and particular nitrogen background gas pressure, precursors are able to interact in a such a way as to allow for the formation of BN film on the surface of the heated substrate.<sup>[32]</sup> The growth rate of the BN film is ≈1 nm growth per 10 laser pulses, and the substrate stage during growth was heated to 200 °C. All depositions were either 50 or 100 nm thick, and following the deposition, the EG samples were characterized again with optical microscopy and Raman spectroscopy (see the Supporting Information). Optical microscopy was performed intermittently throughout the experiment to ensure that various exposures did not damage the samples and then once more after the experiment was completed.

To initially acquire data for both the surface conductivity and the dielectric loss tangent, each sample is incrementally inserted into an air-filled standard R100 rectangular waveguide whose dimensions include a length of 127.0 mm, height of 10.16 mm, and width of 22.86 mm. Please refer to **Figure 1** for a schematic of the experimental setup. In the case of this experiment, the increments are in 0.5 mm steps. The perturbations in the local electric field, which manifest themselves as changes in both frequency and quality (*Q*) factor in the transverse electric field (TE<sub>103</sub>) mode used in the cavity, are measured by a vector network analyzer connected to the waveguide and subsequently recorded by a custom-written LabVIEW<sup>[31]</sup> program. The fundamental theory behind the microwave cavity and its connection to the surface conductivity is well-documented.<sup>[28]</sup> As a brief summary of the result of that derivation, Equation (1) defines some crucial parameters:

$$x = \frac{V_s}{V_0}, \quad y' = \frac{f_0 - f_s}{f_0}, \quad \text{and} \quad y'' = \frac{1}{Q_s} - \frac{1}{Q_0} \quad (1)$$

In Equation (1), quantities with the subscript S pertain to that quantity when the sample is present in the cavity, whereas the subscript zero indicates that the quantity is obtained when the cavity remains unperturbed, with the exception of  $V_s$  and  $V_0$ , which are just the total volumes of the sample and cavity, respectively. The  $f$  is for frequency and  $Q$  is for quality factor. Equations (2) and (3) correspondingly show the real and imaginary components of an expression relating the change in frequency of the cavity TE<sub>103</sub> mode with another expression dependent on the complex dielectric function of the material:

$$y' = 2x(\epsilon_r' - 1) - b' \quad (2)$$

$$y'' = 4x\epsilon_r'' - b'' \quad (3)$$

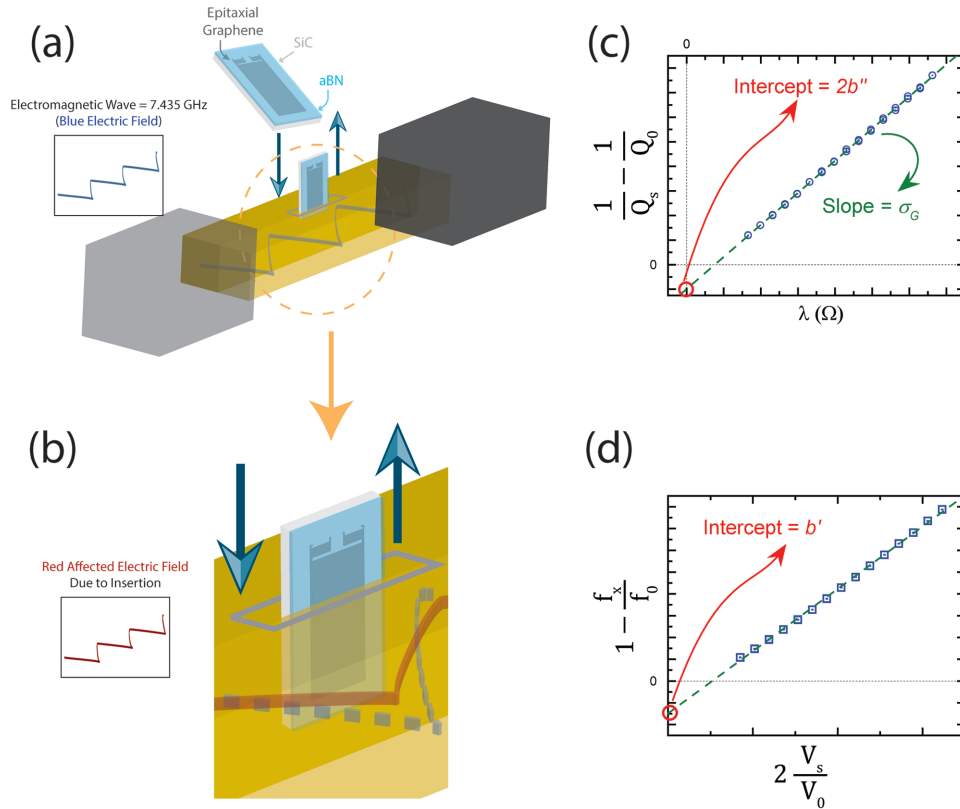


**Figure 1.** a) A schematic of the main experimental setup. The gold region is the waveguide, the black (and transparent black) regions are the couplers which are nearly cross-polarized, and the sample is shown as being inserted into a slot in the center of the waveguide. b) When the sample is inserted, the interaction of the surface charges and the generated electromagnetic waves produces displacement electromagnetic fields which perturb the original waves, recorded as a change in quality factor  $Q$ . c) The changes in  $Q$  factor are plotted as part of an algebraic expression whose slope can be interpreted as the surface conductivity. The  $y$ -intercept can also be interpreted as  $2b''$ . d) Plotting a related expression involving the change in frequency yields a  $y$ -intercept that can be interpreted as  $b'$ . Both  $b'$  and  $b''$  are respectively the real and imaginary portion of the mathematical term that describes the  $TE_{103}$  mode frequency shifts due to nonuniform depolarization fields generated by the inserted sample.

In Equations (2) and (3), the general variable  $b$  is such that  $b^* = b' + ib''$ , where the complex number  $b^*$  represents a contribution to the  $TE_{103}$  mode frequency shift due to nonuniform depolarization fields generated by the inserted sample.<sup>[28]</sup> The dielectric function, or complex permittivity, can be simplified in the imaginary case to  $\epsilon_r'' \approx \epsilon_G''$  because of graphene's dominant dielectric loss compared to SiC.<sup>[29]</sup> Furthermore, the imaginary portion of graphene's dielectric function can be related to the surface conductivity with Equation (4):<sup>[33]</sup>

$$\epsilon_G'' = \frac{\sigma_G}{2\pi\epsilon_0 f_x t_G} \quad (4)$$

Here,  $\sigma_G$  is the surface conductivity of the graphene,  $\epsilon_0$  is the vacuum permittivity,  $f_x$  is the frequency and its subscript  $x$  merely indicates that this quantity depends on how much of the sample is present in the cavity, and  $t_G$  is the thickness of the graphene, which is a quantity that ultimately gets cancelled out in Equation (5), where Equation (3) is rewritten in its fully expanded form:

$$\frac{1}{Q_s} - \frac{1}{Q_0} = \frac{2wh_x f_x}{\pi\epsilon_0 f_0^2 V_0} \sigma_G - 2b'' = \lambda\sigma_G - 2b'' \quad (5)$$

The only remaining variables to define in Equation (5) are the width  $w$  and height  $h_x$  of the graphene that is present in the cavity, where the height is assumed to change while the width is kept fixed. From the fabrication method, the width is known to be 4.04 mm and the total height is known to be 10 mm. For graphical simplicity, the coefficient of the surface conductivity is labeled  $\lambda$ . As mentioned earlier, the sample is lowered into the cavity in 0.5 mm steps, as illustrated in Figure 1. The first point is recorded when the slightest perturbation of the initial frequency, approximately  $7.4350 \times 10^9$  Hz, is detected by the instrument, which translates to approximately one part in  $10^5$  Hz. At each step, the resulting frequency shift and  $Q$  factor is recorded, and the process is repeated until the sample is lowered 10 mm into the cavity. At this point, the entire procedure is reversed and data are collected again at each of the step positions until the sample is fully removed. Upon collecting the data, they are analyzed and plotted in the form of Equation (5) to yield the surface conductivity. An example plot is shown in Figure 1c. From the slope of the plotted data, one can obtain the surface conductivity of the specific graphene sample. From the  $y$ -intercept, the  $2b''$  term can also be obtained, which will become useful in later analyses.

Another descriptive quantity that can be extracted from a similar algebraic manipulation is the dielectric loss tangent.

In essence, the loss tangent is a representation of a material's capacity to dissipate electrical energy into heat. In dielectric materials,  $\tan \delta_e = \frac{\epsilon''}{\epsilon'}$  and it is generally frequency-dependent. However, for graphene, the loss tangent can take on a slowly changing numerical value throughout the small neighborhood of electromagnetic frequency in which the experiment is conducted.<sup>[34,35]</sup> Unlike the imaginary case, the real case requires consideration of the effects of the SiC. Equation (6) shows how the real part of the dielectric function should be expanded to account for the SiC:

$$y' = 2x(\epsilon'_G + \epsilon'_{SiC} - 1) - b' \quad (6)$$

Equation (3) and (6) can be reorganized to isolate  $\epsilon'_G$  and  $\epsilon''_G$ , then divided to yield Equation (7) below:

$$\frac{y'' + 2b''}{2y' + 2b' + 4x(1 - \epsilon'_{SiC})} = \frac{\epsilon''_G}{\epsilon'_G} = \tan \delta_e \quad (7)$$

Although it appears that one must accurately know  $\epsilon'_{SiC}$ , one can eliminate this third term since it is several orders of magnitude smaller than the other two terms in the denominator. Figure 1d shows that the  $b'$  term is extracted from the collected data as a  $y$ -intercept to the line plotted in the form of Equation (2).

Once both quantities are extracted for one sample, that same sample is exposed to a variety of environmental conditions and intermittently measured with the non-contact microwave cavity (i.e., sample is measured, then exposed, then measured, then exposed, and this process is repeated for many different exposures). There are seven different conditions of exposure for which effects on unprotected and encapsulated EG samples are measured. The first condition, labeled as a brown data point, is the deposition of *a*-BN on seven EG samples of which three are coated with 50 nm *a*-BN and four with 100 nm *a*-BN. The second and third conditions are simply ambient air and argon environments, represented by the colors green and purple, respectively. The fourth condition is a cold thermal cycle, represented by the color cyan, during which the sample is placed in a sealed vessel made of two KF blank flanges, held in place by a polytetrafluoroethylene (PTFE or Teflon) chip carrier, and ultimately submerged into a Thermos<sup>[31]</sup> food container filled with liquid nitrogen. Figures S2 and S3, and additional text in the Supporting Information provide simulation snapshots and details on thermal simulations made to estimate the time it would take to cool a graphene sample to approximately 77 K.

The simulation predicted a time of about 22 min, so for any given cold thermal cycle, the cooling process was timed for 30 min. A simulation was also graphed for the warming up process, which involved the placement of the sample vessels in a Thermotron<sup>[31]</sup> testing chamber at 40 °C. The predicted time was approximately 40 min, so the process was run for 45 min for each case. More details regarding the validity of the simulations and a comparison with tests done on a blank SiC chip are provided in the Supporting Information.

The fifth and sixth conditions used for exposure were an environment of 85 °C with 0% relative humidity, marked by red data points, and an environment of 60 °C with 85% relative humidity (marked by orange data points), both of which also involved the use of the Thermotron testing chamber. The seventh and final condition that was utilized was a gold deposition and etch, marked by golden data points. The idea behind the seventh condition was to simulate how EG is fabricated after *a*-BN deposition, and the first step involves

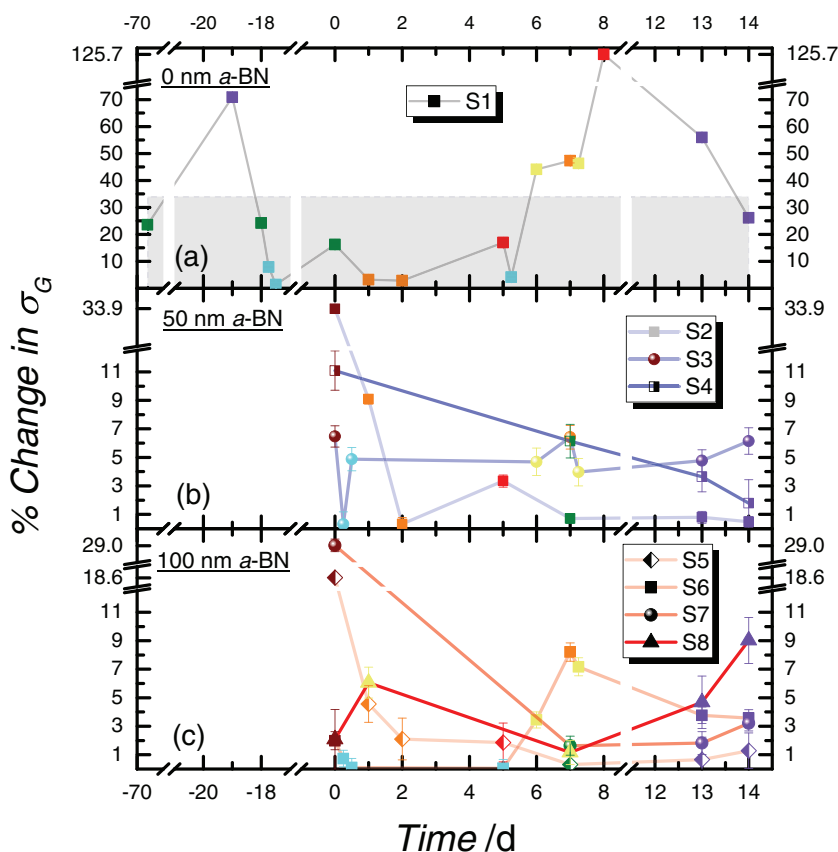


**Figure 2.** The percentage difference of the surface conductivity is taken between the postexposure measurement and the previously measured point. Error bars represent one standard deviation from the linear fit of surface conductivity (see Figure 1c). a) This graph shows the various measurements of the surface conductivity after different types of exposures, where each exposure is represented by a data point with a different color. The shaded region indicates the region in which the vertical axis is zoomed for the 50 and 100 nm samples. b) With the exception of the initial deposition of *a*-BN, a 50 nm encapsulation prevents percentage differences from exceeding 10%. The color, transparency, and style of data point of the curve are only meant to be a guide to the eye for the three different samples with this encapsulation thickness. c) Keeping the vertical axis for the lowest numerical range identical in size and scale as the 50 nm case, the four 100 nm thick *a*-BN samples also retain stable surface conductivity, to within 10% of the previously measured value. Curve transparency and data point style are guides to the eye.

**Table 1.** For data points of varying color, the corresponding exposure type is responsible for causing the percentage change indicated by the data point. These colors are shown below.

Number	Exposure Type	Color
1	Post $\alpha$ -BN deposition	Brown
2	Ambient—22.2 °C, 45% relative humidity	Green
3	Argon gas	Purple
4	Cold thermal cycle	Cyan
5	60 °C, 85% relative humidity	Orange
6	85 °C, 0% relative humidity	Red
7	Gold deposition and aqua regia etch	Gold

a gold deposition. After the various steps of lithography and pattern design which take place while the EG is protected by the gold layer, the final step is always a removal of a fraction of the gold so as to leave an area of the graphene clean and accessible for measuring, whether by optical, electrical, or other means. The gold is etched away by aqua regia diluted with DI water, similar to what is described in Table S2 of the Supporting Information.

As the surface conductivity is collected, the percentage difference is taken between the obtained post-exposure value and the previously obtained, pre-exposure value to gauge how much change was introduced by the selected type of exposure. Immediately after the measurement, the sample is placed in the next type of exposure. **Figure 2** summarizes the behavior of the eight samples, of which one is the unprotected sample, three are the 50 nm  $\alpha$ -BN samples, and four are the 100 nm  $\alpha$ -BN samples. Again, each point is marked by a color representative of the type of exposure that was in use since the previously acquired data point. Those colors can be translated in **Table 1**, noting that the sequential order of the colors on the table does not correspond to the sequential order of exposures selected for the eight samples. As an example, if one follows sample S1, it is noted that after EG growth, a measurement is made, followed by exposure to (and intermittent measurements thereafter): ambient conditions (green), argon gas (purple), ambient (green), cold thermal cycle (cyan), cold thermal cycle (cyan), ambient (green), 60 °C/85% humidity (orange), 60 °C/85% humidity (orange), 60 °C/0% humidity (red), cold thermal cycle (cyan), Au deposition and etch (gold), 60 °C/85% humidity (orange), Au deposition and etch (gold), 60 °C/0% humidity (red), argon gas (purple), and finally argon gas (purple).

What becomes clear is that all exposure types except for the cold thermal

cycle have an impact such that the change in the surface conductivity of the unprotected EG is greater than 10% in some cases and greater than 50% in other cases. Specifically, the argon gas treatment, high temperature and humidity, and aqua regia gold etching have the greatest contributions of change in the unprotected sample. Looking at the encapsulated samples, the vertical axis is scaled to reflect how the changes in the surface conductivity drop considerably for all the exposure types, except for the initial  $\alpha$ -BN deposition itself. The vertical scales in Figure 2b,c are identical for the smallest numerical range, and by comparing the 50 nm samples to the 100 nm samples, not much change occurs. One may argue that the 100 nm data appear to have more points closer to the 0% value than the 50 nm data, but this statement cannot be made absolutely since there are an unequal number of samples with the varying thicknesses. The data show that the average change in surface conductivity for the 50 nm  $\alpha$ -BN is  $3.6\% \pm 0.9\%$  and the average change in surface conductivity for the 100 nm  $\alpha$ -BN is  $3.1\% \pm 1.0\%$ . The overlap in the two averages, within uncertainty, may suggest that the protection offered by  $\alpha$ -BN reaches an asymptotic value at a thickness less than or equal to 50 nm. The style and

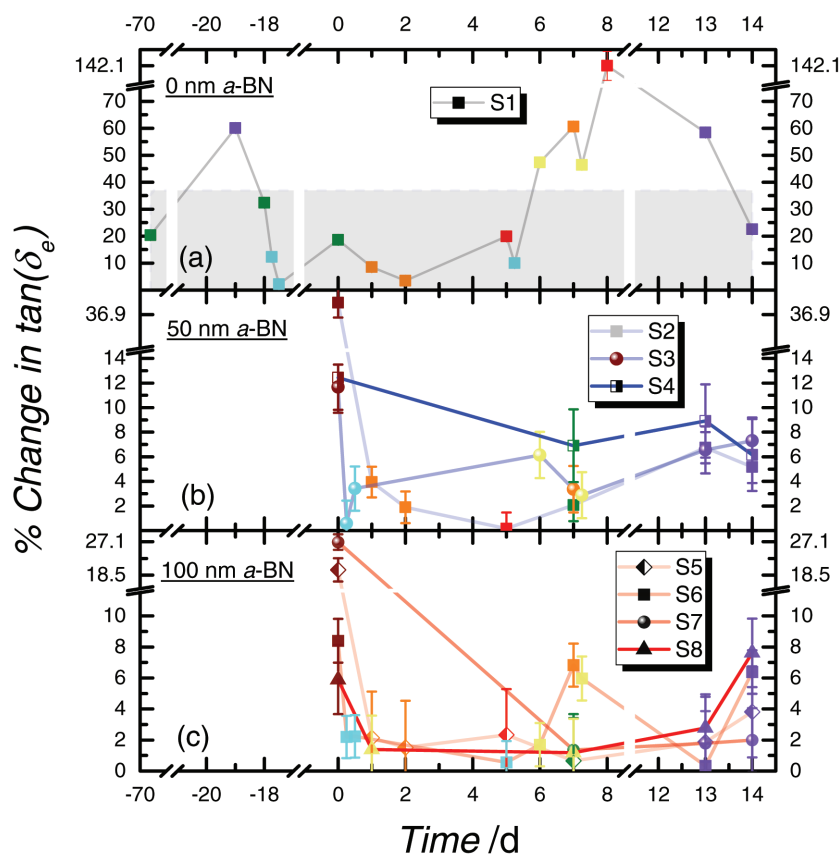


**Figure 3.** The percentage difference of the dielectric loss tangent is taken between the postexposure measurement and the previously measured point. The figure is formatted like Figure 2, where the exposure types are represented by data points of varying color, and within each different thickness of  $\alpha$ -BN, there is a different style of data point corresponding to each sample. Error bars represent uncertainties in the fit parameters after propagation (see Figure 1d for relevant parameter). Although the detailed behavior of the loss tangent is slightly different, the overall trend regarding the stability of this parameter is similar to the surface conductivity for samples coated with a) 0 nm, b) 50 nm, and c) 100 nm  $\alpha$ -BN.

**Table 2.** For each of the eight samples, the initial values following the growth of the EG and then the values following the deposition of *a*-BN are shown below.

Sample Number	S1	S2	S3	S4	S5	S6	S7	S8
Surface Conductivity [ $10^{-4}$ S]	2.06	2.11	2.22	2.16	1.86	2.46	1.53	3.53
Relative Uncertainty [%]	0.797	0.389	0.847	1.488	1.165	0.618	0.962	1.341
Dielectric Loss Tangent	0.0613	0.0620	0.0651	0.0645	0.0549	0.0750	0.0426	0.0865
Relative Uncertainty [%]	3.28	2.56	3.59	5.89	6.08	2.74	4.16	4.51

color of the curves are meant only as a guide to the eye to distinguish between samples.

The dielectric loss tangent is extracted from the data, processed in a similar manner, and presented in **Figure 3**. The general trend is similar to that of the surface conductivity. All exposures beyond the initial *a*-BN deposition have a significantly smaller effect on the loss tangent for samples encapsulated with either 50 nm or 100 nm of *a*-BN. One SiC chip was prepared such that only *a*-BN was present to check the order of magnitude of the conductivity and loss tangent. The contribution to the conductivity is completely negligible, while the contribution to the loss tangent is on the order of  $10^{-4}$ ,<sup>[36]</sup> compared with an absolute graphene loss tangent value on the order of  $10^{-2}$ . In this respect, the *a*-BN layer contributes less than 1%, below the uncertainty for each point.

Regarding both the surface conductivity and dielectric loss tangent, it is found that 50 nm of *a*-BN is sufficient to protect the EG from a variety of environmental or chemical exposure conditions, and furthermore, that this encapsulation method is most effective against exposure to argon, gold, and aqua regia. The level of increased protection from *a*-BN is most negligible in the case where the EG is being thermally cycled from room temperature (300 K) to 77 K, noting that thermal cycling initially had a small change on the two properties of unprotected EG.

To gain insight into the absolute values of the surface conductivity and dielectric loss tangent for each of the eight samples, please refer to **Table 2**, which shows the value of the surface conductivity and the loss tangent before *a*-BN deposition. As an additional supplement, the progression of the absolute values of these two parameters is graphically presented in Figure S5 (Supporting Information). An inventory of samples and their exact exposures are then shown in Figure S6 (Supporting Information) to ensure clarity of which exposures were used for each sample. Additional comments on the immediate application to protected Hall bar devices for QHE measurements are provided in the Supporting Information.

In summary, experimental results are reported on the extraction of the surface conductivity and dielectric loss tangent, whose mathematical relationships are derived with electromagnetic theory (i.e., Maxwell's equations). Data are primarily collected with a noncontact resonance microwave cavity, assembled with an air-filled, standard R100 rectangular waveguide configuration. By using *a*-BN as an encapsulation layer, stability of EG's electrical properties under ambient laboratory conditions is greatly improved. Additionally, samples were exposed to a variety of environmental and chemical conditions. Regarding their effectiveness as an encapsulation material for EG, there are no large differences

between 50 and 100 nm thicknesses of *a*-BN, and both thicknesses are sufficient to preserve surface conductivity and dielectric loss tangent to within 10% of its previously measured value. These results have essential importance in the mass production of millimeter-scale graphene devices because electrical stability can be demonstrated despite chemical fabrication methods, storage, and basic thermal cycling.

## Supporting Information

Supporting Information is available from the Wiley Online Library or from the author.

## Acknowledgements

A.F.R. and H.M.H. would like to thank the National Research Council's Research Associateship Program for the opportunity. The authors would like to thank Art Safriet of University of Dayton Research Institute for the design of components for the *a*-BN growth chamber. The work of C.-I.L. at NIST was made possible by arrangement with Prof. C.-T. Liang of National Taiwan University. Work done by Y.Y. was supported by federal grant #70NANB12H185. H.Y.L. would like to thank Theiss Research for the opportunity. The authors would like to thank Vishal Panchal for fruitful discussions.

## Conflict of Interest

The authors declare no conflict of interest.

- [1] A. K. Geim, K. S. Novoselov, *Nat. Mater.* **2007**, *6*, 183.
- [2] K. S. Novoselov, V. I. Fal'ko, L. Colombo, P. R. Gellert, M. G. Schwab, K. Kim, *Nature* **2012**, *490*, 192.
- [3] K. S. Novoselov, A. K. Geim, S. V. Morozov, D. Jiang, Y. Zhang, S. V. Dubonos, I. V. Grigorieva, A. A. Firsov, *Science* **2004**, *306*, 666.
- [4] Y. Fukuyama, R. E. Elmquist, L.-I. Huang, Y. Yang, F.-H. Liu, N.-H. Kaneko, *IEEE Trans. Instrum. Meas.* **2015**, *64*, 1451.
- [5] M. A. Real, T. Shen, G. R. Jones, R. E. Elmquist, J. A. Soons, A. V. Davydov, *IEEE Trans. Instrum. Meas.* **2013**, *62*, 1454.
- [6] R. Ribeiro-Palau, F. Lafont, J. Brun-Picard, D. Kazazis, A. Michon, F. Cheynis, O. Couturaud, C. Consejo, B. Jouault, W. Poirier, F. Schopfer, *Nat. Nanotechnol.* **2015**, *10*, 965.
- [7] A. Tzalenchuk, S. Lara-Avila, A. Kalaboukhov, S. Paolillo, M. Syväjärvi, R. Yakimova, O. Kazakova, T. J. B. M. Janssen, V. Fal'ko, S. Kubatkin, *Nat. Nanotechnol.* **2010**, *5*, 186.

- [8] T. J. B. M. Janssen, A. Tzalenchuk, R. Yakimova, S. Kubatkin, S. Lara-Avila, S. Kopylov, V. Fal'ko, *Phys. Rev. B* **2011**, *83*, 233402.
- [9] F. Lafont, R. Ribeiro-Palau, D. Kazakis, A. Michon, O. Couturaud, C. Consejo, T. Chassagne, M. Zielinski, M. Portail, B. Jouault, F. Schopfer, W. Poirer, *Nat. Commun.* **2015**, *6*, 6806.
- [10] T. J. B. M. Janssen, S. Rozhko, I. Antonov, A. Tzalenchuk, J. M. Williams, Z. Melhem, H. He, S. Lara-Avila, S. Kubatkin, R. Yakimova, *2D Mater.* **2015**, *2*, 035015.
- [11] B. Jeckelmann, B. Jeanneret, *Rep. Prog. Phys.* **2001**, *64*, 1603.
- [12] A. Hartland, K. Jones, J. M. Williams, B. L. Gallagher, T. Galloway, *Phys. Rev. Lett.* **1991**, *66*, 8.
- [13] Y. Yang, G. Cheng, P. Mende, I. G. Calizo, R. M. Feenstra, C. Chuang, C.-W. Liu, C.-I. Liu, G. R. Jones, A. R. Hight Walker, R. E. Elmquist, *Carbon* **2017**, *115*, 229.
- [14] S. Novikov, N. Lebedeva, K. Pierz, A. Satrapinski, *IEEE Trans. Instrum. Meas.* **2015**, *64*, 1533.
- [15] T. Ciuk, O. Petruk, A. Kowalik, I. Jozwik, A. Rychter, J. Szmids, W. Strupinski, *Appl. Phys. Lett.* **2016**, *108*, 223504.
- [16] M. W. K. Nomani, V. Shields, G. Tompa, N. Sbrockey, M. G. Spencer, R. A. Webb, G. Koley, *Appl. Phys. Lett.* **2012**, *100*, 092113.
- [17] Y. Yang, L.-I. Huang, Y. Fukuyama, F.-H. Liu, M. A. Real, P. Barbara, C.-T. Liang, D. B. Newell, R. E. Elmquist, *Small* **2015**, *11*, 90.
- [18] T. O. Wehling, K. S. Novoselov, S. V. Morozov, E. E. Vdovin, M. I. Katsnelson, A. K. Geim, A. I. Lichtenstein, *Nano Lett.* **2008**, *8*, 173.
- [19] Z. H. Ni, H. M. Wang, Z. Q. Luo, Y. Y. Wang, T. Yu, Y. H. Wu, Z. X. Shen, *J. Raman Spectrosc.* **2009**, *41*, 479.
- [20] S. Lara-Avila, K. Moth-Poulsen, R. Yakimova, T. Bjørnholm, V. Fal'ko, A. Tzalenchuk, S. Kubatkin, *Adv. Mater.* **2011**, *23*, 878.
- [21] J. A. Robinson, M. LaBella, K. A. Trumbull, X. J. Weng, R. Cavellero, T. Daniels, Z. Hughes, M. Hollander, M. Fanton, D. Snyder, *ACS Nano* **2010**, *4*, 2667.
- [22] N. Y. Garces, V. D. Wheeler, J. K. Hite, G. G. Jernigan, J. L. Tedesco, N. Nepal, C. R. Eddy Jr., D. K. Gaskill, *J. Appl. Phys.* **2011**, *109*, 124303.
- [23] M. J. Hollander, M. LaBella, Z. R. Hughes, M. Zhu, K. A. Trumbull, R. Cavallero, D. W. Snyder, X. Wang, E. Hwang, S. Datta, J. A. Robinson, *Nano Lett.* **2011**, *11*, 3601.
- [24] J. M. P. Alaboson, Q. H. Wang, J. D. Emery, A. L. Lipson, M. J. Bedzyk, J. W. Elam, M. J. Pellin, M. C. Hersam, *ACS Nano* **2011**, *5*, 5223.
- [25] N. R. Glavin, C. Muratore, M. L. Jespersen, J. Hu, P. T. Hagerty, A. M. Hilton, A. T. Blake, C. A. Grabowski, M. F. Durstock, M. E. McConney, D. M. Hilgert, T. S. Fisher, A. A. Voevodin, *Adv. Funct. Mater.* **2016**, *26*, 2640.
- [26] M. S. Bresnehan, M. J. Hollander, M. Wetherington, M. Labella, K. A. Trumbull, R. Cavallero, D. W. Snyder, J. A. Robinson, *ACS Nano* **2012**, *6*, 5234.
- [27] N. R. Glavin, M. L. Jespersen, M. H. Check, J. Hu, A. M. Hilton, T. S. Fisher, A. A. Voevodin, *Thin Solid Films* **2014**, *572*, 245.
- [28] N. D. Orloff, J. Obrzut, C. J. Long, T. Lam, P. Kabos, D. R. Novotny, J. C. Booth, J. Alexander Liddle, *IEEE Trans. Microwave Theory Tech.* **2014**, *62*, 2149.
- [29] J. Obrzut, C. Emiroglu, O. Kirillov, Y. Yang, R. E. Elmquist, *Measurement* **2016**, *87*, 146.
- [30] L. Hao, J. Gallop, S. Goniszewski, O. Shaforost, N. Klein, R. Yakimova, *Appl. Phys. Lett.* **2013**, *103*, 123103.
- [31] Commercial equipment, instruments, and materials are identified in this paper in order to specify the experimental procedure adequately. Such identification is not intended to imply recommendation or endorsement by the National Institute of Standards and Technology or the United States government, nor is it intended to imply that the materials or equipment identified are necessarily the best available for the purpose.
- [32] N. R. Glavin, C. Muratore, M. L. Jespersen, J. Hu, T. S. Fisher, A. A. Voevodin, *J. Appl. Phys.* **2015**, *117*, 165305.
- [33] C. J. F. Botcher, P. Bordewijk, *Theory of Electric Polarization*, Elsevier Science, Amsterdam, The Netherlands **1996**.
- [34] L. F. Chen, C. K. Ong, C. P. Neo, V. V. Varadan, V. K. Varadan, *Micro-wave Electronics: Measurement and Materials Characterization*, Wiley, Hoboken, NJ, USA **2004**.
- [35] K. Rubrice, X. Castel, M. Himdi, P. Parneix, *Materials* **2016**, *9*, 825.
- [36] J. Iglesias, W. B. Westphal, *Supplementary Dielectric Constants and Loss Measurements on High Temperature Materials*, MIT, Cambridge, MA, USA **1967**.

Received: February 9, 2017  
Revised: April 18, 2017  
Published online: